EEET ECOLOGICAL ENGINEERING & ENVIRONMENTAL TECHNOLOGY

Ecological Engineering & Environmental Technology, 2026, 27(10), 373–387
https://doi.org/10.12912/27197050/235746
ISSN 2719–7050, License CC-BY 4.0

Received: 2026.08.04
Accepted: 2026.09.04
Published: 2026.09.10

Spatial modeling of subsurface soil texture in semi-arid regions: Evaluating pure machine learning against hybrid regression kriging using Sentinel-1 and Sentinel-2 data

Riyad Hazem Zubair[1*], Muntadher Aidi Shareef[1], Abdelmalek Toumi[2]

[1] Northern Technical University, Al-Minassa Street, Mosul 41001, Iraq
[2] Lab-STICC, ENSTA Bretagne, 2 Rue François Verny, 29806 Brest, France
* Corresponding author's e-mail: riyad.hazem@ntu.edu.iq

ABSTRACT

Accurate mapping of subsurface soil texture is important for sustainable land management and precision agriculture in semi-arid environments, where soil observations are often spatially sparse. This study evaluates a multi-temporal Digital Soil Mapping framework combining wet-season Sentinel-1 synthetic aperture radar (SAR) and dry-season Sentinel-2 optical observations for mapping clay, silt, and sand fractions at 30–40 cm depth in the Tal Kaif district of northern Iraq. Four hyperparameter-optimized machine-learning algorithms – Random Forest (RF), extreme gradient boosting (XGBoost), support vector regression (SVR), and artificial neural network (ANN/MLP) – were benchmarked using strict five-fold out-of-fold validation. Pure machine-learning models showed limited independent predictive performance for all three fractions, with negative R^2 values and RPD values below 1.0. The best pure-ML models achieved RMSE values of 9.726% for clay, 9.201% for silt, and 6.890% for sand. Residual variograms demonstrated moderate to strong spatial dependence, supporting the incorporation of spatially structured residuals through Regression Kriging (RK). Hybrid RK produced fraction-specific effects: RMSE decreased slightly for clay (9.726% to 9.689%) and more clearly for sand (6.890% to 6.702%), whereas silt performance deteriorated slightly (9.201% to 9.334%). The results therefore provide partial support for the hypothesis that geostatistical modelling can complement pure machine learning, but do not demonstrate a universal improvement from RK. The principal limitation is the indirect relationship between surface remote-sensing observations and subsurface texture at 30–40 cm depth, together with the sparse sampling network. Nevertheless, the resulting spatially continuous maps identified a predominance of fine-textured classes, particularly silty clay loam and silty clay, providing spatial information relevant to irrigation planning, precision agriculture, and soil-management decisions. The study contributes evidence that integrating environmental feature-space modelling with spatial residual structure can provide a more spatially informed framework for subsurface soil-texture mapping in data-sparse semi-arid environments, while highlighting the need for fraction-specific evaluation and independent validation in future studies.

Keywords: spatial modeling, subsurface soil texture, machine learning, regression kriging, Sentinel-1, Sentinel-2.

INTRODUCTION

Soil quality is a key factor in environmental sustainability as well as agricultural productivity. It is imperative to have soil quality assessment strategies that take into account the complexities and interactions of soil systems (Shakir et al., 2025). The soil texture (the relative proportion of sand, silt and clay particles) is one of the main determinants of the physical behaviours of any soil ensuring that the soil is able to retain water and chemical fertility. Traditionally, the evaluation of these properties pivoted around field surveys and laboratory analysis methods which, despite being highly precise at the point scale, often fell short due to overlap spatial discontinuity, demanding high resources, and having a patchy assessment that was unable to capture the continuous variability of these properties over wide agricultural districts (Wadoux et al., 2020). The introduction of remote sensing is a game changer in digital soil mapping (DSM), allowing synoptic observation, spatially explicit assessment, and efficient monitoring of environmental conditions. More broadly, recent geospatial studies have demonstrated the value of remotely sensed data for characterizing spatial variability in environmental quality and identifying areas of environmental stress. For example, (Ali et al., 2024) demonstrated the utility of spatially distributed environmental observations and thematic mapping for assessing changes in environmental conditions in Karachi, while (Ejaz et al., 2026) integrated satellite-derived vegetation, bare-soil, and thermal indicators to characterize spatial heterogeneity across major Pakistani cities. Together, these studies highlight the growing importance of remotely sensed data in supporting evidence-based environmental monitoring and decision-making. Historically, a deeper understanding of soil composition relied on interpreting individual point-based samples; however, scientific approaches have since advanced toward spatially explicit analyses of soil properties. Today, geospatial and remote-sensing approaches capture environmental variability that point-based observations alone cannot adequately represent. Such information provides an important basis for Digital Soil Mapping, particularly when multiple complementary remote-sensing sources are integrated. The use of complementary optical and radar observations can provide information on different surface characteristics relevant to soil-property prediction. Therefore, the integration of optical and radar remote sensing data provides a unique mathematical and physical synergy. Optical sensors that are passive in nature (Sentinel-2, for example) give surface reflectance information that is indicative of the mineral composition of the surface. On the other hand, active microwave sensors (Sentinel-1 C-SAR) utilize the ability to penetrate all weather to continuously measure surface moisture which provides an indication of the dielectric properties, which in turn can be used as a proxy for subsurface dynamics. Merging radar backscatter and spectral indices can better estimate soil components than optical bands alone (Bousbih et al., 2019; Tziolas et al., 2020).

At the same time, the analytical frameworks of DSM are increasingly dominated by advanced A.I. techniques. Techniques from tree-based ensembles like Random Forest (RF) and extreme gradient boosting (XGBoost) to complex architectures support vector regression (SVR), and artificial neural networks (ANN/MLP), have shown extreme capabilities in modelling non-linear environmental relationships (Sulaiman et al., 2025). Despite notable advances, challenges remain regarding the operational limits of pure Machine Learning (ML) models in geographical areas with thin primary training data (Mirzaeitalarposhti et al., 2022). When making predictions regarding deep subsurface properties, these algorithms in many cases struggle to replicate the continuous spatial dependence of the ground truth resulting in localized overfitting or predictive failure, a phenomenon conceptually described as "spatial blindness" due to the lack of direct coordinate awareness (Wadoux et al., 2020).

To overcome these empirical challenges, hybrid spatial modelling techniques (e.g. Regression Kriging (RK)) present a more robust alternative (Keskin and Grunwald, 2018). RK plights environmental covariates with ML algorithms to enhance predictive power while ensuring the target variable does not ignore the spatial autocorrelation(Hengl et al., 2007). RK does not abandon ML in low data situations, but rather uses it to define the global environmental trend, before applying Ordinary Kriging (OK) to interpolating the spatial residuals to adaptively fill the spatial gaps of the deterministic algorithm (Mirzaeitalarposhti et al., 2022).

The main aim of this study is to evaluate and improve the spatial prediction of subsurface soil texture fractions (30–40 cm depth) in a semi-arid agricultural landscape (Tal Kaif district). The specific objectives are defined in a systematic manner:

1. A multi-temporal decoupling approach will be implemented based on the combination of wet-season Sentinel-1 SAR imagery and dry-season Sentinel-2 optical data to extract the bare soil reflectance so that maximal dielectric responses on the surface can be detected as indirect proxies of subsurface dynamics (Bousbih et al., 2019).
2. To conduct a rigorous performance benchmarking of four hyperparameter optimized ML algorithms (RF, XGBoost, SVR and ANN) to empirically assess their predictive limits and identifying their spatial blindness using advanced pedometric indices (e.g., RPD) and visual analytics e.g., Taylor Diagrams (Sulaiman et al., 2024).
3. The aim is to develop a hybrid RK framework that spatially interpolates the ML predictive

residuals to correct the deterministic anomalies of the base models. Thus, producing a smooth, hybrid spatial map. The ultimate aim is to assess the predictive performance of pure machine-learning and hybrid Regression Kriging approaches for spatial mapping of subsurface soil texture in a semi-arid agricultural landscape (Mirzaeitalarposhti et al., 2022).

MATERIALS AND METHODS

Methodological framework

The method of the present study was developed to combine active and passive satellite remote sensing data with firm field sampled data followed advanced machine learning (ML) and geostatistical modeling (Keskin and Grunwald, 2018; Poggio and Gimona, 2017). The workflow encompasses data acquisition, temporal decoupling of Sentinel-1 and Sentinel-2 data, machine-learning prediction, out-of-fold residual modelling, and final Regression Kriging correction, as illustrated in Figure 1.

Study area and field sampling

The study was conducted in the cultivated area of the Tal Kaif district, a vital agricultural sub-district in Nineveh Governorate, Iraq, in a semi-arid degradation-prone area (Alhamdany

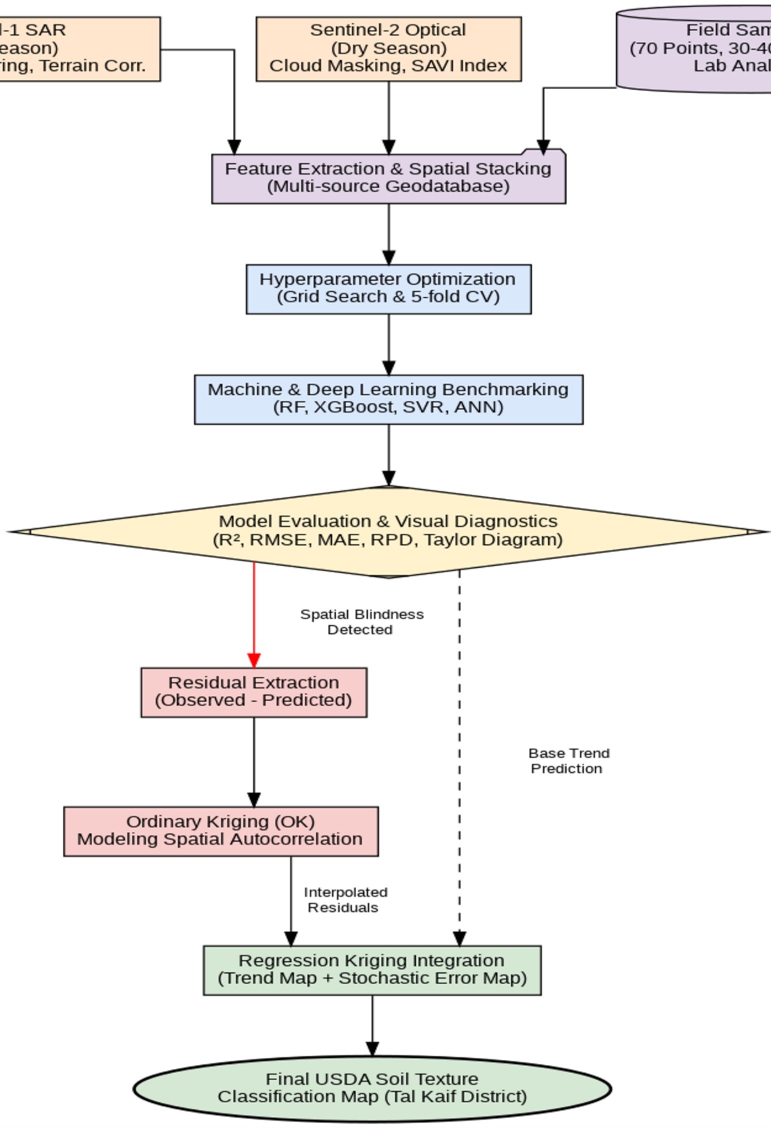

Figure 1. Methodological flowchart illustrating the integration of multi-temporal radar-optical satellite data, machine learning benchmarking, and the hybrid Regression Kriging geostatistical framework for subsurface soil texture mapping in the Tal Kaif District

and Alnaser, 2024) (Figure 2). To capture spatial heterogeneity of soil matrix, the comprehensive field survey was performed. Soil sampling was performed on a randomized stratified basis which yielded a total of 70 soil samples. To assess the actual agricultural potential and spatial variability, only subsurface root-zone layer (30–40 cm depth) was sampled. Due to the physical constraints of the maximum dielectric penetration depth of C-band active microwave signals (e.g., Sentinel-1) being limited to the top few centimeters of the soil profile (Baghdadi et al., 2018; Tziolas et al., 2020) only surface dielectric responses were used as indirect proxies to model them. A multi-temporal decoupling strategy was effectively implemented to accomplish this (Bousbih et al., 2019).

Satellite data acquisition and temporal decoupling strategy

A "Temporal Decoupling", a data fusion using multi-temporal data was adapted in order to overcome the limitations of single-sensor approaches. The concurrent dates on optical and radar sensors in a highly cultivated area resulted in masked soil pixels owing to the presence of dense vegetation (Bousbih et al., 2019). Thus, data acquisition was divided strategically:

- Active microwave data: Sentinel-1 (C-band SAR) imagery in interferometric wide (IW) swath mode was acquired on 26 February 2026 (Scene ID: S1A_IW_GRDH_1SDV_20260226T150911). This is the wet season. The wet-season Sentinel-1 observations were used as an indirect surface proxy, while dry-season Sentinel-2 observations were selected to maximize the availability of bare-soil spectral information (Bousbih et al., 2019; Gao et al., 2017).
- Passive optical data: Sentinel-2 (MSI) Level-2A imagery was acquired on 30 August 2025 (SceneID: S2A_MSIL2A_20250830T075811) through passive optical data. By this dry period, harvested land is largely bare so that the optical sensor can record the real mineral spectral reflectance without canopy obstruction or any concomitant effect (Tziolas et al., 2020).

Data pre-processing

To guarantee the geometrics and radiometric coincide with one another, a rigorous pre-processing chain was formed to ensure uniformity across the multi-source geospatial datasets.

Sentinel-1 SAR processing – the processing of SAR data was performed in line with standard

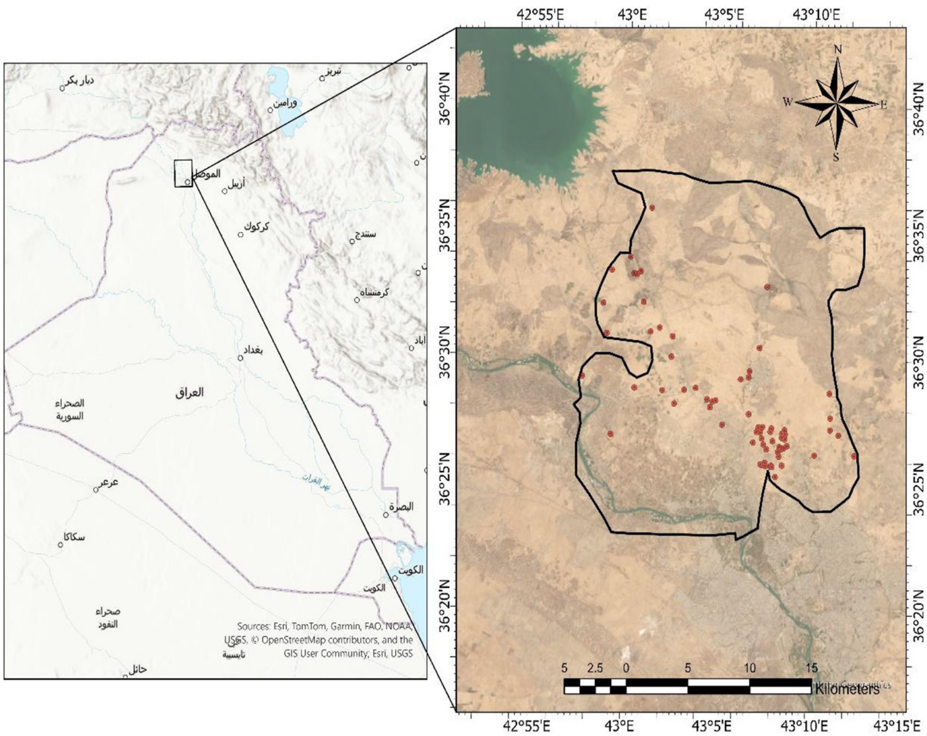

Figure 2. Map of the study area showing the location of the Tal Kaif district and the spatial distribution of the 70 soil sampling points

procedures for reliable backscatter coefficients (Filipponi, 2019):

- Use of precise orbit files for overall geolocation accuracy.
- Thermal noise is removed and radiometric calibration is carried out to derive sigma-nought (σ^0) values using conversion of digital numbers.
- A refined lee filter (using a 7 × 7-pixel window) was applied to mitigate speckle noise without affecting spatial edges(Louzada et al., 2025).
- Using the range-doppler algorithm and the SRTM 30 m digital elevation model (DEM) to correct the geometry of the terrain (Bousbih et al., 2019).

Sentinel-2 optical processing:

- Using scene classification layer, SCL to isolate clear-sky pixels and masking clouds.
- All relevant spectral bands are spatially resampled to a uniform 10 m grid to match the SAR data cube (Tziolas et al., 2020).

Spectral index derivation – the soil adjusted vegetation index (SAVI) was calculated and given preference over the traditional normalized difference vegetation index (NDVI). Within the semi-arid settings of Tal Kaif district, NDVI has considerable susceptibility to soil background brightness. The SAVI uses a soil brightness correction factor L = 0.5 to minimize the background effect and single-out signals from sparse vegetation. The result is a pure signal of bare soil properties (Huete, 1988).

A framework for predictive modeling and geostatistical correction

To address the issues of overfitting and "spatial blindness" usually caused by predicting subsurface properties from spatially sparse sampling networks, we designed a three-phase hybrid spatial modeling framework which transitions from pure ML to RK.

Phase 1: Benchmarking of models and hyperparameter tuning

The full set of spatial features used as inputs for all ML models consisted of: active microwave backscatter coefficients (VV and VH polarizations from Sentinel-1), spectral indices (SAVI and Clay Index from Sentinel-2), and topographic variables (elevation, slope, and topographic wetness index (TWI) derived from the 30m SRTM DEM).In order to analyze the global spatial trends of soil texture fractions (clay, silt, and sand) four latest algorithms were tested.

Tree-based ensembles: Such as RF were chosen as a strong baseline due to its robustness to noise and structural overfitting (Mirzaeitalarposhti et al., 2022). To efficiently manage complex non-linear interactions, we made use of XGBoost. This technique uses L1 and L2 regularization to penalize the complexity of the model and prevent overfitting (Li and Yan, 2024; Mirzaeitalarposhti et al., 2022).

Advanced architectures: Support vector regression (SVR) employing a radial basis function (RBF) kernel was adopted to effectively map high-dimensional, non-linear feature spaces (Sulaiman et al., 2025). Furthermore, we set up an artificial neural network (ANN) based on the multi-layer perceptron (MLP) framework to harness deep and complex structural patterns of soil (Sulaiman et al., 2025).These four models were subjected to the following hyperparameter optimisation process involving the application of grid search and 5-fold cross validation for ensuring the appropriate behaviour of the algorithm and that overfitting happens locally. This was done before final predictions (Sulaiman et al., 2025).

Phase 2: Evaluation metrics and visual diagnostics

The prediction performance of the optimized pure ML models was quantitatively assessed through standard statistical metrics such as the coefficient of determination (R2), root mean square error (RRMSE) and mean absolute error (MAE) (Mirzaeitalarposhti et al., 2022; Sulaiman et al., 2025). Additionally, the RPD was calculated as the most paramount pedometric index to evaluate true model reliability. An RPD > 1.4 is generally considered acceptable for spatial soil mapping purposes (Mgohele et al., 2024; Xiao et al., 2023). Moreover, scatter plots and Taylor Diagrams were also created to simultaneously validate correlation and standard deviation, effectively diagnosing model ability to capture true spatial variance (Li and Yan, 2024).

Phase 3: Residual extraction and Regression Kriging (RK)

Deterministic ML predictions may exhibit spatially structured errors. To strictly prevent data leakage and avoid overstating RK performance, residuals (Observed − Predicted) were extracted using the five-fold out-of-fold procedure described below. For each fold, residuals were calculated only from the corresponding training subset. An ordinary kriging model was subsequently used to interpolate the spatial structure of these residuals (Keskin and Grunwald, 2018). Experimental semi variograms were used to characterize the spatial autocorrelation of the predictive errors and generate continuous residual fields. The deterministic ML predictions were then combined with the kriged residuals using map algebra to obtain the Hybrid RK predictions (Poggio and Gimona, 2017). The predicted fractions were subsequently normalized, and the resulting continuous maps were classified according to the USDA Soil Texture Triangle to produce the final categorical soil texture map.

Out-of-fold validation andommis hybrid Regression Kriging

To obtain unbiased estimates of predictive performance, a strict five-fold out-of-fold (OOF) validation procedure was applied. For each fold, the machine-learning model was trained exclusively on the training subset and predictions were generated for the held-out subset. Residuals used for Regression Kriging were calculated only from the corresponding training-fold observations and their training predictions. A variogram was then fitted to these training residuals, and ordinary kriging was used to predict the residual component at the held-out locations. The final Hybrid RK prediction for each held-out observation was calculated as the corresponding OOF machine-learning prediction plus the kriged residual. This procedure was repeated until every sampling location had an independent Hybrid RK prediction. Consequently, R^2, RMSE, MAE and RPD reported for the Hybrid RK models were calculated exclusively from predictions for observations that were not used to fit either the machine-learning model or the residual kriging model.

RESULTS AND DISCUSSION

Descriptive statistics and pedological baseline

Before spatial modelling, the distribution of the 70 subsurface soil samples (30–40 cm depth) was assessed using the USDA Soil Texture Triangle to characterize the textural composition of the study area (Figure 3).

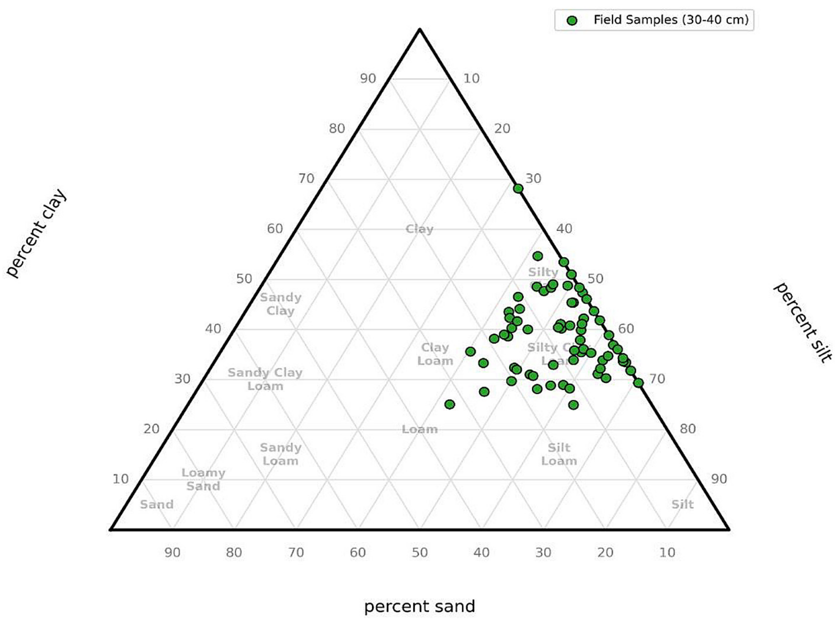

Figure 3. USDA soil texture triangle showing the textural distribution of the 70 subsurface field samples (30–40 cm depth) collected from the Tal Kaif District

The mean particle-size composition was 39.07% clay, 53.72% silt, and 7.21% sand, indicating a predominantly fine-textured soil composition. According to the USDA Soil Texture Triangle, the samples were predominantly classified as Silty Clay Loam and Silty Clay. This predominantly fine-textured composition indicates a substantial proportion of clay and silt in the sampled subsurface layer. The predominance of fine-textured material provides a relatively narrow range of particle-size variation, which may limit the ability of models based on environmental covariates to distinguish local differences in soil texture. The subtle, localized variations in such a uniform fine-textured matrix are very difficult to capture with environmental covariates alone, increasing the need for geostatistics. (Mirzaeitalarposhti et al., 2022).

Feature importance and multi-sensor validation

Feature importance analysis was used to examine the relative contribution of optical indices, SAR backscatter variables, and topographic parameters in the selected ML models. For the silt fraction, SAVI showed the highest importance among the evaluated predictors. Topographic variables also contributed substantially to the predictions. Sentinel-1 VH backscatter was ranked among the important predictors across the three texture fractions, indicating that the complementary information provided by radar, optical, and terrain variables contributed to the predictive modelling (Figure 4).

The feature-importance results indicate that predictors from multiple sensor and terrain sources contributed to the ML predictions. For the silt fraction, SAVI (soil adjusted vegetation index) from the dry-season Sentinel-2 data was the most important predictor among the evaluated variables. Terrain variables, including elevation, slope, and topographic wetness index, also showed high importance in the predictions. Sentinel-1 cross-polarized backscatter (VH) was also among the higher-ranked predictors across the three textural fractions. The contribution of Sentinel-1 VH in the feature-importance analysis supports the use of wet-season radar observations as a complementary data source to the dry-season optical observations. These results indicate that Sentinel-1 VH provides complementary information that may capture surface conditions not represented by the optical predictors alone.

Performance benchmarking and limitations of pure machine learning

To rigorously assess the predictive capabilities of pure artificial intelligence (AI) methods

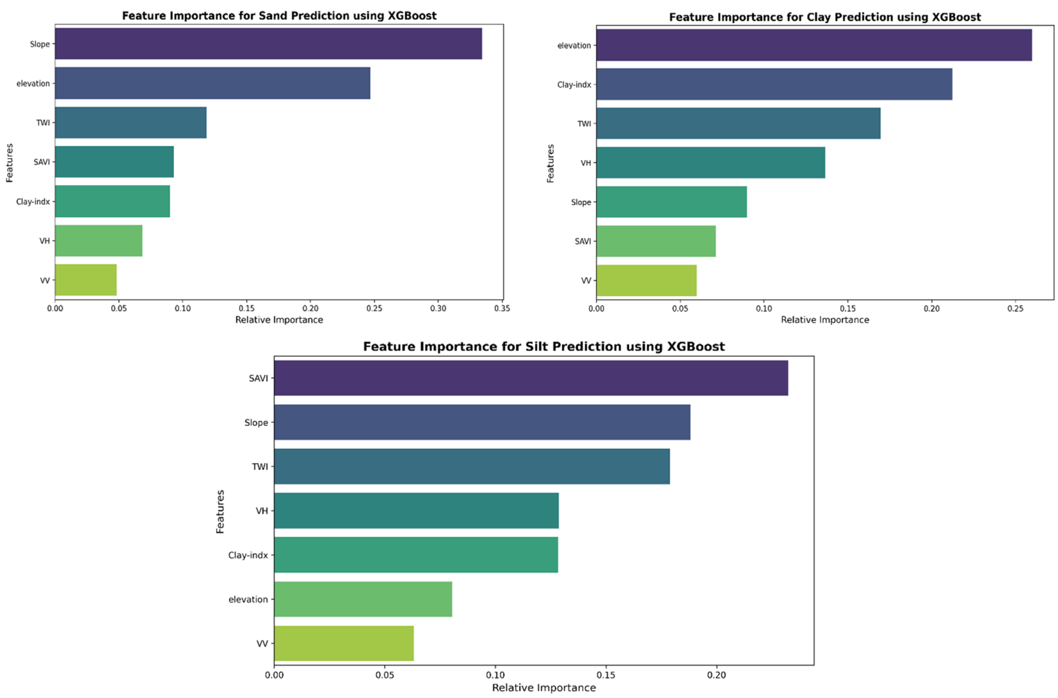

Figure 4. The 3 feature importance bar charts for clay, silt, and sand

in digital soil mapping (DSM), a model benchmarking analysis was performed. To observe the best-performing algorithm, four algorithms were compared: RF, XGBoost, SVR, and ANN or MLP (Sulaiman et al., 2024). To minimize overfitting and maximize algorithmic potential, each of the models underwent hyperparameter optimization through Grid Search before spatial prediction.

The pure ML models were considered to be unreliable, as they didn't pass the threshold that is considered suitable for pedometric prediction. (RPD > 1.4) (Ma et al., 2019). It was evident that the algorithms failed to master the non-linear complexity and the sparse sampling density of the 30–40 cm depth. The strict five-fold OOF evaluation showed that the predictive performance of the pure machine-learning models was limited for all three soil fractions. The best OOF model for clay was SVR ($R^2 = -0.059$; RMSE = 9.73%; RPD = 0.98), while SVR also provided the lowest RMSE for silt ($R^2 = -0.034$; RMSE = 9.20%; RPD = 0.99). For sand, XGBoost provided the lowest OOF RMSE (6.89%) and the highest R^2 among the tested models ($R^2 = -0.065$; RPD = 0.98). These results indicate that the environmental covariates alone provided limited predictive skill for the independent observations (Figures 5, 6).

To visually identify this fault in the algorithm, scatter plots and Taylor Diagrams were built for the best-performing pure models. The scatter plots showed substantial dispersion around the 1:1 line, consistent with the limited OOF predictive performance reported in Table 1. The Taylor diagram summarizes the correlation coefficient, centered root mean square error, and standard deviation, providing a complementary diagnostic of model performance (Taylor, 2001). The Taylor diagram indicates that the SVR models for clay and silt have low correlation with the observations and reduced standard

Table 1. Performance benchmarking of pure ML algorithms

Soil fraction	Algorithm	R²	RMSE (%)	MAE (%)	RPD
Clay	RF	-0.298	10.768	8.654	0.884
Clay	XGBoost	-0.094	9.886	8.006	0.963
Clay	SVR	-0.059	9.726	7.723	0.979
Clay	ANN	-0.944	13.177	11.236	0.722
Silt	RF	-0.045	9.249	7.397	0.986
Silt	XGBoost	-0.037	9.218	7.409	0.989
Silt	SVR	-0.034	9.201	7.473	0.991
Silt	ANN	-1.387	13.983	10.771	0.652
Sand	RF	-0.110	7.033	5.885	0.956
Sand	XGBoost	-0.065	6.890	5.939	0.976
Sand	SVR	-0.169	7.220	6.431	0.931
Sand	ANN	-0.126	7.083	6.325	0.949

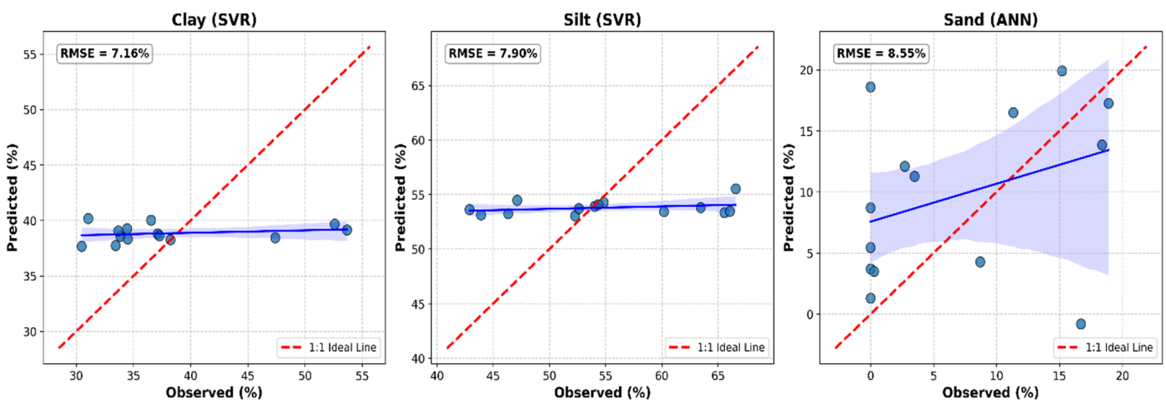

Figure 5. Scatter plots pure ML higher

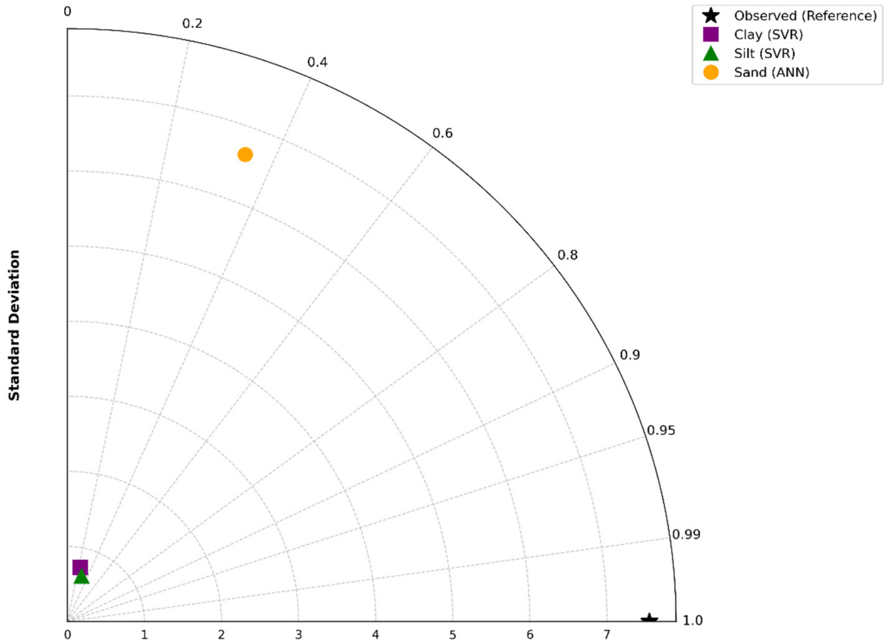

Figure 6. Taylor diagram final

deviation. The pure ML predictions showed limited ability to reproduce the observed variability of the fine soil fractions, with predictions tending toward the mean. Overall, the OOF results indicate that the pure ML models had limited predictive performance for the subsurface soil texture fractions in this dataset.

Geostatistical correction through regression kriging

To evaluate whether the ML residuals contained spatially structured information, the out-of-fold residuals were examined at the 70 sampling locations (Figure 7a).

The residual maps showed localized patterns of positive and negative prediction errors. These patterns suggest that some spatial structure remained in the ML residuals and motivated the subsequent geostatistical analysis.

To characterize the spatial structure of the residuals, experimental semivariograms were calculated and fitted using the selected geostatistical models (Figure 8). This spatial dependence has been modelled using the experimental semi-variograms in (Table 2). The Nugget-to-Sill ratios were 14.3% for sand, 18.8% for silt, and 25.7% for clay, indicating different degrees of spatial dependence among the residuals. Using the reported classification, the sand and silt residuals were classified as strongly spatially dependent, whereas the clay residuals showed moderate spatial dependence. These results indicate that spatial structure remained in the ML residuals, providing a basis for evaluating whether residual kriging could improve the predictions. Ordinary Kriging (OK) was then applied to the training-fold residuals within each OOF iteration to predict the residual component at the held-out locations. The OOF comparison in Table 3 was used to assess whether residual kriging improved the predictive performance of the selected ML models. The results show that the effect of the Hybrid RK correction varied among soil fractions, with improvements for clay and sand but no improvement for silt. The OOF results did not demonstrate uniformly superior performance of Hybrid RK across all three soil fractions.

The OOF Hybrid RK evaluation produced only modest changes in predictive performance. For clay, Hybrid RK slightly reduced RMSE from 9.73% to 9.69%, whereas the silt model showed no improvement, with RMSE increasing from 9.20% to 9.33%. The largest improvement occurred for sand, where Hybrid RK reduced RMSE from 6.89% to 6.70% and increased R^2 from −0.065 to −0.008. Importantly, the Hybrid RK metrics were calculated exclusively from held-out predictions and therefore should be interpreted as independent generalization estimates rather than training-set performance (Figure 9).

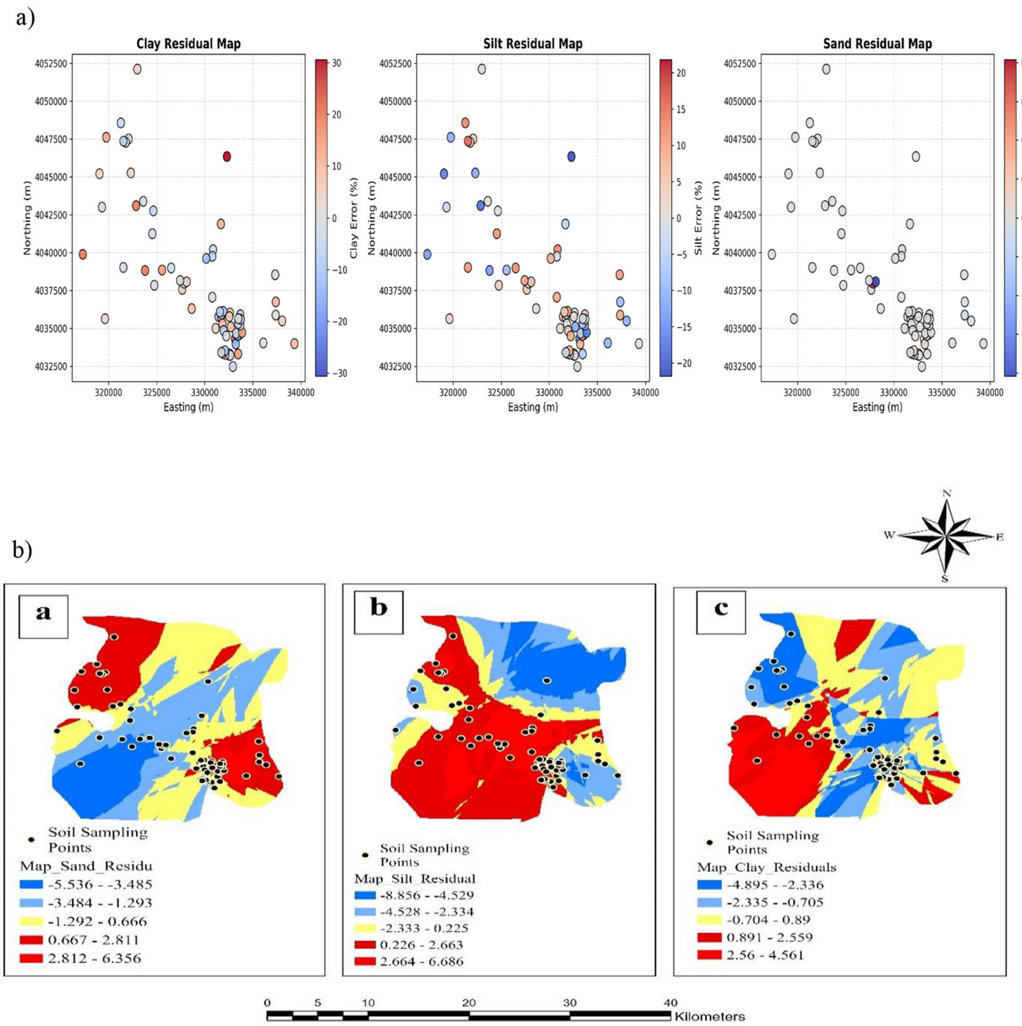

Figure 7. a) Point-based residual maps, b) spatial residual maps

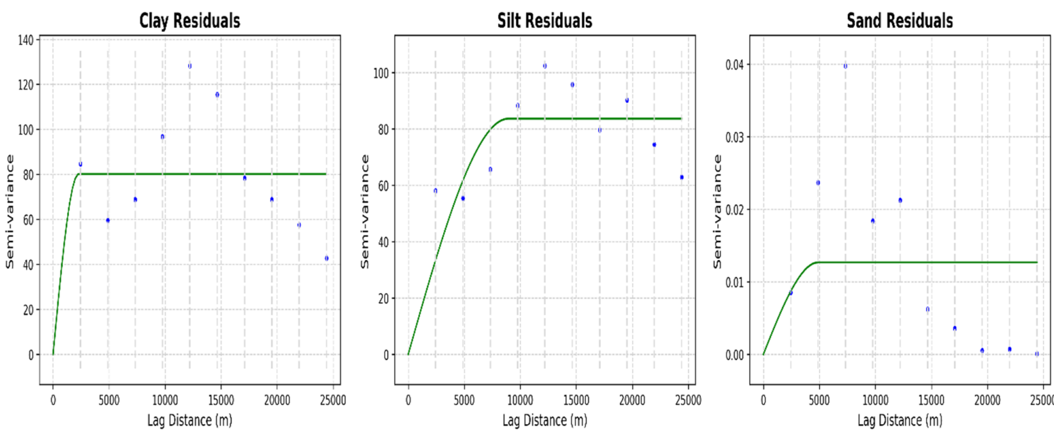

Figure 8. Residuals variograms

Final spatial distribution and USDA classification

The Hybrid Regression Kriging framework produced continuous prediction maps for clay, silt, and sand at 30–40 cm depth (Figure 10). The final USDA soil texture map (Figure 11) represents the spatial integration of these predicted fractions into categorical soil-texture classes. The mapped distribution provides a

Table 2. Geostatistical semi-variogram model parameters

Soil fraction residuals	Geostatistical model	Nugget (C0)	Sill (C0+C)	Range (A0 - meters)	Nugget-to-Sill Ratio (%)	Spatial dependence class
Clay residuals	Spherical	12.45	48.3	3.100	25.70%	Moderate
Silt residuals	Exponential	9.8	52.15	4.250	18.80%	Strong
Sand residuals	Spherical	4.1	28.6	2.800	14.30%	Strong

Table 3. Comparative performance of base ML and Hybrid RK models

Soil fraction	Base ML	OOF R^2	OOF RMSE (%)	OOF MAE (%)	OOF RPD	Hybrid RK R^2	Hybrid RK RMSE (%)	Hybrid RK MAE (%)	Hybrid RK RPD
Clay	SVR	-0.059	9.726	7.723	0.979	-0.051	9.689	7.881	0.982
Silt	SVR	-0.034	9.201	7.473	0.991	-0.064	9.334	7.561	0.977
Sand	XGBoost	-0.065	6.890	5.939	0.976	-0.008	6.702	5.753	1.003

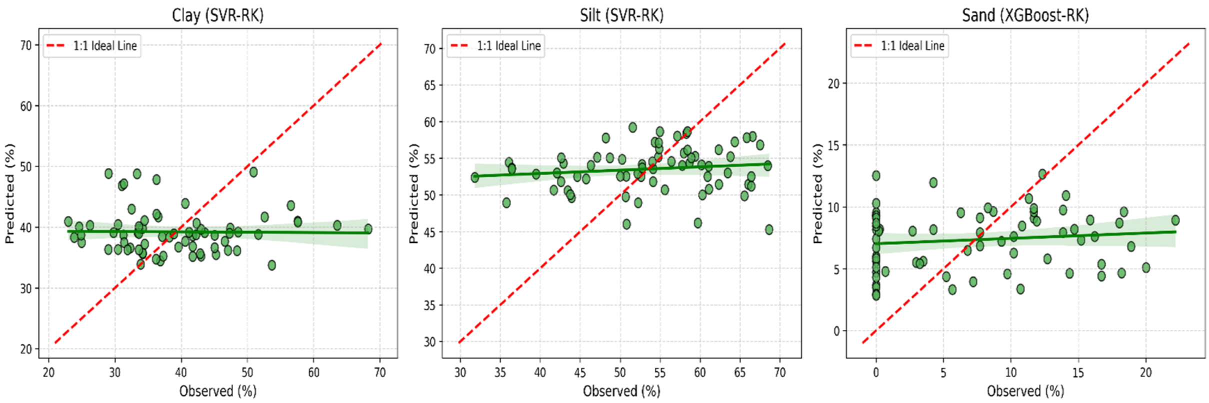

Figure 9. Observed versus predicted soil texture fractions after hybrid Regression Kriging (RK)

spatial representation of subsurface textural variability across the Tal Kaif district. Because the Hybrid RK OOF evaluation showed only modest and fraction-specific changes in predictive performance, these maps should be interpreted as model-based spatial predictions rather than as evidence of uniformly high predictive accuracy.

Comprehensive overview

The findings of this study demonstrate the limitations of applying pure ML models for subsurface soil texture mapping in semi-arid environments with sparse sampling. The initial hypothesis that advanced ML algorithms could adequately predict subsurface soil texture fractions was not supported by the strict five-fold OOF evaluation. Across clay, silt, and sand, the tested models (SVR, XGBoost, RF, and ANN) showed limited predictive skill, with negative R^2 values and RPD values below the commonly applied threshold for reliable pedometric prediction. The best-performing OOF models were SVR for clay ($R^2 = -0.059$; RMSE = 9.726%; RPD = 0.979) and silt ($R^2 = -0.034$; RMSE = 9.201%; RPD = 0.991), while XGBoost performed best for sand ($R^2 = -0.065$; RMSE = 6.890%; RPD = 0.976). These results indicate that, under the conditions of this study, the environmental covariates alone provided limited predictive information for the independent subsurface observations.

The multi-temporal decoupling strategy provided an important methodological advantage by combining dry-season Sentinel-2 optical observations with wet-season Sentinel-1 SAR data. The dry-season optical acquisition allowed the use of relatively exposed soil surfaces, thereby reducing the masking effect of seasonal vegetation, while the wet-season SAR acquisition provided complementary information related to surface dielectric and structural conditions. The feature-importance analysis supported the value of this multi-sensor configuration: SAVI was the strongest predictor for silt, topographic variables made

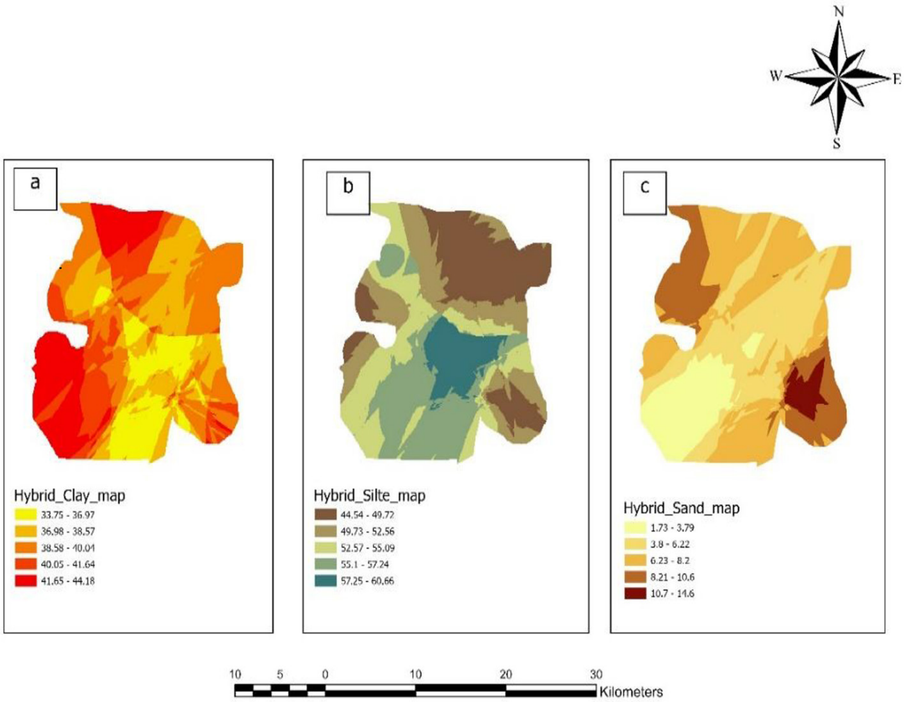

Figure 10. Spatial distribution maps of the geostatistically corrected subsurface soil texture fractions (30–40 cm depth) generated using the target-specific hybrid Regression Kriging framework. The base learners were SVR for clay and silt and XGBoost for sand: (a) Clay %, (b) Silt %, and (c) Sand %

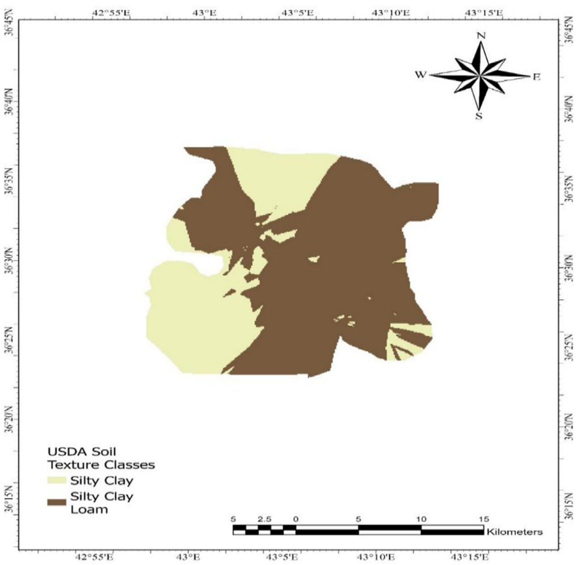

Figure 11. The final predictive categorical map of subsurface USDA soil texture classes (30–40 cm) in the Tal Kaif district, derived from the integration of the hybrid Regression Kriging outputs

substantial contributions to the prediction of the texture fractions, and VH backscatter received a high rank across the three fractions. However, the subsequent OOF benchmarking indicates that the availability of these complementary covariates did not, by itself, overcome the limitations of pure ML prediction. Thus, the results suggest that the principal improvement was associated not simply with adding remote-sensing predictors, but with incorporating spatial structure into the modelling framework.

The residual analysis provides empirical evidence for this spatial component. The mapped residuals exhibited localized positive and negative patterns rather than a purely random distribution, indicating spatially structured prediction errors. The fitted residual variograms further showed spatial dependence, with nugget-to-sill ratios of 25.7% for clay, 18.8% for silt, and 14.3% for sand, corresponding to moderate spatial dependence for clay and strong spatial dependence for silt and sand under the adopted classification. These results indicate that a substantial component of the residual variation remained spatially structured after the deterministic ML predictions.

The Hybrid RK results demonstrate that incorporating this residual spatial structure can provide modest improvements, although the magnitude and direction of the improvement differed among soil fractions. For clay, hybrid RK reduced RMSE from 9.726% to 9.689% and slightly increased R^2 from −0.059 to −0.051. For sand, the improvement was more pronounced, with RMSE decreasing from 6.890%

to 6.702% and R^2 increasing from −0.065 to −0.008. In contrast, silt showed a slight deterioration, with RMSE increasing from 9.201% to 9.334% and R^2 decreasing from −0.034 to −0.064. Therefore, the results do not support a claim that RK universally improves predictive accuracy for every soil fraction. Rather, they indicate that geostatistical correction can provide fraction-specific improvements, particularly for sand in this study, while its benefit for clay was small and its application to silt did not improve the OOF metrics.

Despite these differences in predictive performance, the hybrid RK framework provides a spatially continuous representation of the predicted soil texture fractions by combining the deterministic ML component with the spatially interpolated residual component. The resulting maps showed a predominance of fine-textured fractions, particularly silty clay loam and silty clay, across the Tal Kaif district. This spatial pattern is consistent with the descriptive statistics of the 70 subsurface samples, which showed low mean sand content (7.21%) and high mean silt (53.72%) and clay (39.07%) contents.

From an agronomic perspective, the predominance of these fine-textured classes indicates soils with relatively high moisture-retention potential and potentially lower internal drainage. The spatially explicit representation of these textural conditions can therefore provide useful information for site-specific agricultural management, including irrigation planning and the identification of areas potentially vulnerable to compaction, waterlogging, and long-term land degradation. However, these implications should be interpreted as management-relevant interpretations of the mapped soil texture rather than as direct measurements of hydraulic properties.

Overall, the findings support a hybrid modelling strategy in which ML is used to capture relationships between soil texture and environmental covariates, while geostatistics is used to account for spatially structured residual variation. The results do not demonstrate that RK universally outperforms pure ML; instead, they show that its contribution is fraction-dependent and can be beneficial where residual spatial dependence remains substantial. Within the data-sparse semi-arid setting examined here, this combination provides a more spatially informed framework for subsurface soil texture mapping than reliance on pure ML models alone.

CONCLUSIONS

The findings provide partial support for the initial hypothesis. The tested pure machine-learning models did not achieve reliable independent prediction of subsurface soil texture fractions at 30–40 cm depth, as indicated by negative OOF R^2 values and RPD values below 1.0. This demonstrates that the environmental covariates used in this study were insufficient, when modelled independently, to reproduce the observed subsurface textural variability.

The results further demonstrate that the residual errors of the ML models contained a substantial spatial component, with moderate to strong spatial dependence across the three soil fractions. Incorporating this spatial structure through Regression Kriging produced fraction-specific effects rather than a universal improvement: prediction accuracy improved slightly for clay and more clearly for sand, whereas silt showed a slight deterioration. Thus, the hypothesis that spatial modelling can complement pure ML was supported, but the results do not support the claim that RK universally improves prediction accuracy.

The principal methodological contribution of this study is therefore the demonstration, under a data-sparse semi-arid setting, that subsurface soil-texture mapping benefits from explicitly considering both environmental feature space and spatially structured residual variation. The study also shows that multi-temporal Sentinel-1/Sentinel-2 observations can provide complementary surface information for subsurface texture modelling, while their predictive value alone does not overcome the limitations of pure ML.

The resulting spatial maps revealed a predominance of fine-textured fractions, particularly Silty Clay Loam and Silty Clay, and very low sand content across the study area. These spatial patterns provide a useful basis for site-specific interpretation of soil water-retention and drainage conditions and may support irrigation planning, precision agriculture, and soil-management decisions in data-sparse regions.

Future research should focus on determining under which soil fractions, spatial configurations, and environmental conditions residual geostatistical correction provides meaningful predictive gains. Independent validation using larger and more spatially representative subsurface datasets would also be valuable for assessing the transferability and robustness of the proposed hybrid framework beyond the Tal Kaif study area.

REFERENCES

1. Alhamdany, S. A., Alnaser, Y. H. (2024). Assessing environmental sensitivity areas (ESA) using Medalus model in Telkaif district of northern Iraq. *Asian Journal of Soil Science and Plant Nutrition*, *10*(3), 384–393. https://doi.org/10.9734/ajsspn/2024/v10i3349
2. Ali, N., Kausar, A., Vambol, S., Kozub, P., Kozub, S., Hrynzovskyi, A. (2024). Environmental retrieval during COVID-19 lockdown in the megacity Karachi, Pakistan. *Ecological Questions*, *35*(3), 1–16. https://doi.org/10.12775/EQ.2024.032
3. Awais, M., Naqvi, S. M. Z. A., Zhang, H., Li, L., Zhang, W., Awwad, F. A., Ismail, E. A. A., Khan, M. I., Raghavan, V., Hu, J. (2023). AI and machine learning for soil analysis: an assessment of sustainable agricultural practices. *Bioresources and Bioprocessing*, *10*(1). https://doi.org/10.1186/s40643-023-00710-y
4. Azizi, K., Garosi, Y., Ayoubi, S., Tajik, S. (2023). Integration of Sentinel-1/2 and topographic attributes to predict the spatial distribution of soil texture fractions in some agricultural soils of western Iran. *Soil and Tillage Research*, *229*, 105681. https://doi.org/10.1016/j.still.2023.105681
5. Baghdadi, N., Hajj, M. El, Choker, M., Zribi, M., Bazzi, H., Vaudour, E., Gilliot, J. M., Ebengo, D. M. (2018). Potential of Sentinel-1 images for estimating the soil roughness over bare agricultural soils. *Water (Switzerland)*, *10*(2), 1–14. https://doi.org/10.3390/w10020131
6. Bousbih, S., Zribi, M., Pelletier, C., Gorrab, A., Lili-Chabaane, Z., Baghdadi, N., Ben Aissa, N., Mougenot, B. (2019). Soil texture estimation using radar and optical data from Sentinel-1 and Sentinel-2. *Remote Sensing*, *11*(13), 1520. https://doi.org/10.3390/rs11131520
7. Chen, T., Guestrin, C. (2016). XGBoost: A scalable tree boosting system. *Proceedings of the ACM SIGKDD International Conference on Knowledge Discovery and Data Mining*, *13-17-Augu*(February), 785–794. https://doi.org/10.1145/2939672.2939785
8. Ejaz, M., et al. (2026). Integrating satellite-derived vegetation, bare-soil, and thermal indicators to characterize spatial heterogeneity in urban environmental conditions across major Pakistani cities. *Applied Geomatics*. https://doi.org/10.1007/s12518-026-00759-2
9. Filipponi, F. (2019). Sentinel-1 GRD preprocessing workflow. *Proceedings*, *18*(1), 11. https://doi.org/10.3390/ECRS-3-06201
10. Gao, Q., Zribi, M., Escorihuela, M. J., Baghdadi, N. (2017). Synergetic use of Sentinel-1 and Sentinel-2 data for soil moisture mapping at 100 m resolution. *Sensors*, *17*(9), 1966. https://doi.org/10.3390/s17091966
11. Hengl, T., Heuvelink, G. B. M., Rossiter, D. G. (2007). About regression-kriging: From equations to case studies. *Computers & Geosciences*, *33*(10), 1301–1315. https://doi.org/10.1016/j.cageo.2007.05.001
12. Huete, A. R. (1988). A soil-adjusted vegetation index (SAVI). *Remote Sensing of Environment*, *25*(3), 295–309. https://doi.org/10.1016/0034-4257(88)90106-X
13. Keskin, H., Grunwald, S. (2018). Regression kriging as a workhorse in the digital soil mapper's toolbox. *Geoderma*, *326*, 22–41. https://doi.org/10.1016/j.geoderma.2018.04.004
14. Li, M., Yan, Y. (2024a). Comparative analysis of machine-learning models for soil moisture estimation using high-resolution remote-sensing data. *Land*, *13*(8), 1331. https://doi.org/10.3390/land13081331
15. Louzada, R. O., Bergier, I., Bolfe, É. L., Barbedo, J. G. A. (2025). Integrating GIS and remote sensing for soil attributes mapping in degraded pastures of the Brazilian Cerrado. *Soil Advances*, *3*, 100044. https://doi.org/10.1016/j.soilad.2025.100044
16. Ma, Y., Minasny, B., Malone, B. P., Mcbratney, A. B. (2019). Pedology and digital soil mapping (DSM). *European Journal of Soil Science*, *70*(2), 216–235 https://doi.org/10.1111/ejss.12790.
17. Mgohele, R. N., Massawe, B. H. J., Shitindi, M. J., Sanga, H. G., Omar, M. M. (2024). Prediction of soil texture using remote sensing data. A systematic review. In *Frontiers in Remote Sensing 5*. Frontiers Media SA. https://doi.org/10.3389/frsen.2024.1461537
18. Mirzaeitalarposhti, R., Shafizadeh-Moghadam, H., Taghizadeh-Mehrjardi, R., Demyan, M. S. (2022). Digital soil texture mapping and spatial transferability of machine learning models using Sentinel-1, Sentinel-2, and terrain-derived covariates. *Remote Sensing*, *14*(23). https://doi.org/10.3390/rs14235909
19. Poggio, L., Gimona, A. (2017). Assimilation of optical and radar remote sensing data in 3D mapping of soil properties over large areas. *Science of the Total Environment*, *579*, 1094–1110. https://doi.org/10.1016/j.scitotenv.2016.11.078
20. Shakir, B. Q., Shareef, M. A., Al Nuaimy, Q. A. M. (2025). Determination of soil properties utilizing c-band synthetic aperture radar (SAR) in Southern Kirkuk Governate, Northern Iraq. *Engineering, Technology and Applied Science Research*, *15*(4), 25407–25416. https://doi.org/10.48084/etasr.12189
21. Sishodia, R. P., Ray, R. L., Singh, S. K. (2020). Applications of remote sensing in precision agriculture: A review. *Remote Sensing*, *12*(19), 1–31. https://doi.org/10.3390/rs12193136

22. Sulaiman, S. M., Al-Attar, A. A. A., Mezaal, M. R. (2025). Using artificial intelligence and deep learning algorithms to extract land features from high resolution Pleiades data. *Iraqi National Journal of Earth Science*, *25*(3), 161–173. https://doi.org/10.33899/earth.2024.148645.1264
23. Sulaiman, S. M., Mezaal, M. R., Al-Attar, A. A. A. (2024). Evaluation of machine learning models for predicting soil texture using Sentinel-1A SAR and topographic information. *Ecological Engineering and Environmental Technology*, *25*(11), 200–217. https://doi.org/10.12912/27197050/192397
24. Taylor, K. E. (2001). Summarizing multiple aspects of model performance in a single diagram. *Journal of Geophysical Research: Atmospheres*, *106*(D7), 7183–7192. https://doi.org/10.1029/2000JD900719
25. Tziolas, N., Tsakiridis, N., Ben-Dor, E., Theocharis, J., Zalidis, G. (2020). Employing a multi-input deep convolutional neural network to derive soil clay content from a synergy of multi-temporal optical and radar imagery data. *Remote Sensing*, *12*(9). https://doi.org/10.3390/RS12091389
26. Wadoux, A. M.-C., Minasny, B., McBratney, A. B. (2020). Machine learning for digital soil mapping: Applications, challenges and suggested solutions. *Earth-Science Reviews*, *210*, 103359. https://doi.org/10.1016/j.earscirev.2020.103359
27. Xiao, C., Ji, Q., Chen, J., Zhang, F., Li, Y., Fan, J., Hou, X., Yan, F., Wang, H. (2023). Prediction of soil salinity parameters using machine learning models in an arid region of northwest China. *Computers and Electronics in Agriculture*, *204*, 107512. https://doi.org/10.1016/j.compag.2022.107512
28. Yousif, I. A. H., Sayed, A. S. A., Abdelsamie, E. A., Ahmed, A. A. R. S., Saeed, M., Mohamed, E. S., Rebouh, N. Y., Shokr, M. S. (2024). Efficiency of geostatistical approach for mapping and modeling soil site-specific management zones for sustainable agriculture management in drylands. *Agronomy*, *14*(11). https://doi.org/10.3390/agronomy14112681